# Tunable Optical filters Using Etched Polarization Maintaining Fiber Hybrid Sagnac Interferometer

**Raisan M. Taher[1] and Tahreer S. Mansour[1,*]**

*Corresponding author: Tahreer@ilps.uobaghdad.edu.iq*

*1- Institute of Laser for Postgraduate Studied, University of Baghdad, Baghdad, Iraq.*

**Abstract:** In modern optical communication system, noise rejection multiple access interference (MAI) must be rejected in dense access network (DAN). This paper will study the dual optical band pass and notch filters. They will be extracted with tunable FWHM using 10cm (PMF) with different cladding diameters formed with etching 125μm PMF after immersing it with 40% of hydrofluoric acid (HF). This fiber acts as assessing fiber to perform Sagnac interferometer with splicing regions that placed 12cm (SMF) for performing hybrid Sagnac interferometer that consists of Mach-Zehnder instead of Sagnac loop which is illuminated by using laser source with centroid wavelength of 1546.7nm and FWHM of 286 pm or 9 ns in the time domain. . Firstly, Three PMF with the same lengths but with different etching durations (10, 20 and 30) min. Secondly, each of these PMFs with different etching durations will affected under tunable stressing forces (10, 20, 50 and100) g applying on cross sectional area and two weights of (5, 10, 25 and 50) g putting on both micro splicing area separately. The minimum FWHM of dual optical band pass and notch filters at specific etching time with mechanical forces getting the best values equal to 123pm and 90pm, respectively. The study found that the HSI interferometer can be used efficiently as a narrow notch filter in integrated optical communication systems since it has high sensitivity in the pm range.

**Keywords**: polarization maintaining fiber (PMF), single mode fibers (SMF), hybrid Sagnac interferometer (HSI), FWHM, dual band pass filter, notch filter.

## 1. Introduction

The generation of ultra-short pulses (USPs) has received a lot of interest among researchers due to the fact that these pulses find potential applications in different fields of science, engineering and medicine [1, 2]. Interferometers have distinctive features such as small size, compactness, noise reduction, bandwidth optimization, simple and low coast implementation capabilities [3, 4], high sensitivity, fast response and immunity to electromagnetic field interference [5]. There are multiple forms of optical fiber interferometers, estimating the fiber Fabry–Pérot interferometer [1], Mach–Zehnder interferometer, Sagnac interferometer and the Michelson [6]. Hybrid inline fiber interferometers accentuate recently as they can enhance sensitivity to sub-pm range, as well as the possibility of selecting best scheme for compact hybrid inline fiber interferometers for the required application [7, 8]. The polymer optical fiber sensor pumped by $CO_2$ laser and achieved strain sensitivity of 28 pm/με [9]. However, there are some drawbacks in the above mentioned interferometers such as complex constructions [7]. Optical fiber-based sensing systems not only require optical band-rejection filters; all-optical signal processing, and optical microwave signal generation also do.

Especially, the notch optical fiber-based filters with limited rejection bandwidths, these are significantly preferred to enhance the detection limit of sensors and enlarge the sensing range [10]. Many intrinsic advantages such as electrically passive operation, remote sensing capability and immunity to electromagnetic interference [11–14]. Several configurations have been employed, such as fiber Bragg gratings (FBGs) [15, 16]. In 2015, Fahad M. Abdulhussein, et al. used two schemes for simultaneous measurements sensors, the first one is with dual FBGs peaks. Every FBG acts as sensing head. The first peak was used for temperature sensing and the obtained sensitivity is 10 pm/°C and the second peak was used for temperature and pressure measurements with sensitivities 9.2 pm/°C and 67 pm/ bar for temperature and pressure respectively [17, 18]. OFIs including Fabry-Perot interferometers (FPIs) [18–21], Mach-Zehnder interferometers (MZIs) [22–24] and fiber. Sagnac interferometers (FSIs) [25, 26] are good candidates for highly sensitive temperature sensors. The applied forces imposed stress on the fiber caused elongation in the length of the fiber. The amount of the fiber elongation can be calculated using equations (1) (2), (3) [27].

$$The\ strain = \frac{\Delta L}{L} = \frac{stress}{young\ modulus} \quad (1)$$

$$stress = \frac{Force\ (N)}{Area(m^2)} \quad (2)$$

$$F = m \times G \quad (3)$$

Where: L, is the original length and fixed, $\Delta L$ is the change in length, F, is the force applied in (N), A, is the cross sectional area in (m², ), m, is the value of the standard weight mass used to induce mechanical force and G, is the gravitational acceleration. In previous our group studies, the micro splicing regions will be acts as a double convex lenses made from one materials (fused Silica), which produced collapse of splicing regions, so mechanical force will be changed focal length of the convex lenses. But the mechanical force that applied on cross sectional area will made filter elongations ($\Delta L$) that measures in micro strain [28].

Young's modulus is the modulus of elasticity ranges from 66 Gpa to 74 Gpa for the SiO2 i.e. 70 Gpa [29].

After converting weights to force, the mechanical forces in this work were done by applying different forces (0.098, 0.196, 0.49, and 0.98) (N) on the interferometer micro–cavities cross sectional area and applied (0.049, 0.098, 0.245, 0.49) (N) on the micro cavity splicing regions of Pm-MZI.

## 2. Experimental setups

The hybrid Sagnac interferometer which consists of Mach-Zehnder instead as a loop that means two micro cavity splicing regions (MCSRs), and connected MZI by FC-SC adapter to the coupler 2×2 which will make Sagnac interferometer. Figure (1) shows the schematic diagram for the experimental setup for the tunable singe PM-Mach Zehnder Sagnac interferometer. one cavity length (Lc) connected in the loop of Sagnac interferometer, the PMF had etched with the hydrofluoric acid (HF) of 40 % concentration, for (10, 20 and 30) min adding to case without etching. Then mechanical forces were varied from (10, 20, 50, and 100) g applied on the cross sectional area and to splicing regions separately with various weights (5, 10, 25, and 50) g.
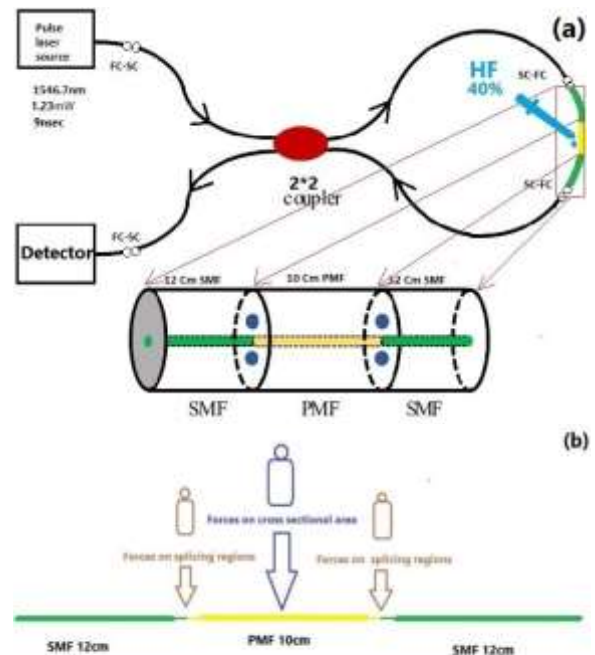


**Figure (1):** schematic diagram of (a) Sagnac with loop PM-MZI (b) how forces applied on cross sectional area and splicing region separately.

The length of Sagnac interferometer totally (2.34m). And get more details about etching time with HF shows in Figure (2).
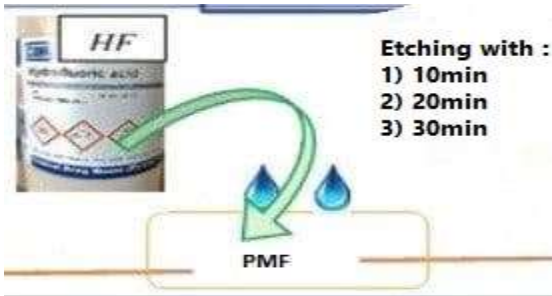
**Figure (2):** the stages of etching with HF of 40 % concentration.

In this experiment, an optical pulse laser source launched to PM-Mach Zehnder Sagnac interferometer. PM-MZI was building by using PMF with the same lengths and different etching times, each of states will give different results according to change in mechanical forces as shown in figure (3).



**Figure (3):** The experimental setup for Sagnac interferometer with loop MZI- PM.

The thickness of PMFs cladding is varying according to etching time of the PMF by 40% of HF with durations (10, 20 and 30) min as shown in table (1), it measured by microscope with 40 X magnifications.

**Table (1):** Fiber diameter with respect to etching time.

| Time of etching (min) | Fiber diameter as a function of etching (μm) |
|---|---|
| 10 | 112.393 |
| 20 | 72.532 |
| 30 | 69.651 |

## 3. Results and discussions

The results divided into two parts, the first part is the relationship between the forces which applied on both cross sectional area and micro-cavities splicing regions with FWHM of dual band pass and notch filters. The second part regarding the effects of etching PMF with different times on the previous results under the same tuning.

The FWHM using HSI with PMF-MZ (as loop) got different results. The minimum FWHM for dual band pass and notch filters are 123 pm, 90 pm respectively when etching at 10min with affecting by weights 100g on cross sectional area and same result was found when use etching at 10min with affecting by weights 10g on both splicing regions. The maximum FWHM for dual band pass and notch filters is 315pm, 125pm respectively was achieved by etching at 20min PMF and affected by weights 50g on cross sectional and the same result was found when using etching at 20min PMF and affected by weights 25g on both splicing regions. All these results shown in the table (2).

**Table (2):** maximum and minimum value of FWHM according to etching and stress.

| Etching PM (min) | Force (N) | FWHM of dual band pass filter (pm) | FWHM of notch filter (pm) |
|---|---|---|---|
| 10 | 0.098 on splicing regions | 123 | 90 |
| 10 | 0.98 on cross area | 123 | 90 |
| 20 | 0.245 on splicing regions | 315 | 125 |
| 20 | 0.49 on cross area | 315 | 125 |

Due to the high sensitivity of the interferometers, the experimental results of the hybrid Sagnac interferometer with loop PM-MZI under the effect of PM fiber etching for three different cladding diameters adding to original diameter before etching showed optical notches occurring in the optical FWHM of the input laser after getting out of interferometer, this promising result opens the door on using it as a very narrow optical notch pass filter.

All these results will show by the FBGA interrogator as a visualizer.

The effect of two types of filter appeared in the output of setup because PMF has zero PMD (polarization mode dispersion) but this effect disappear by using long SMF (1m) or three paddles PC, so different SMF has large polarization mode dispersion (PMD) but PMF has zero (PMD), which can controlled by its beat length BL
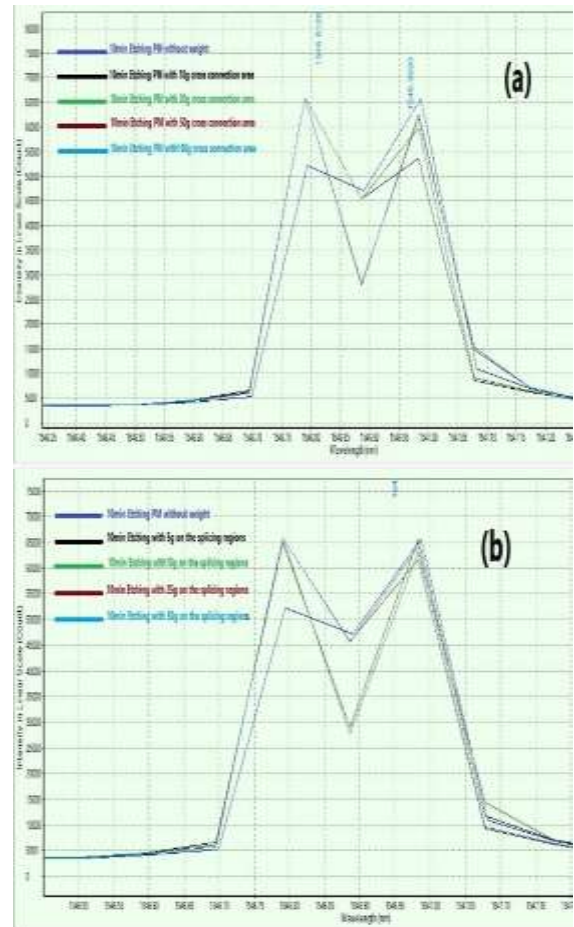
The first case using the PM without etching and applied the mechanical stress as shown in figure (4) which show signals and FHWM of dual band pass filter in the range (126 – 285) pm, and notch filter in range (95 – 114) pm.
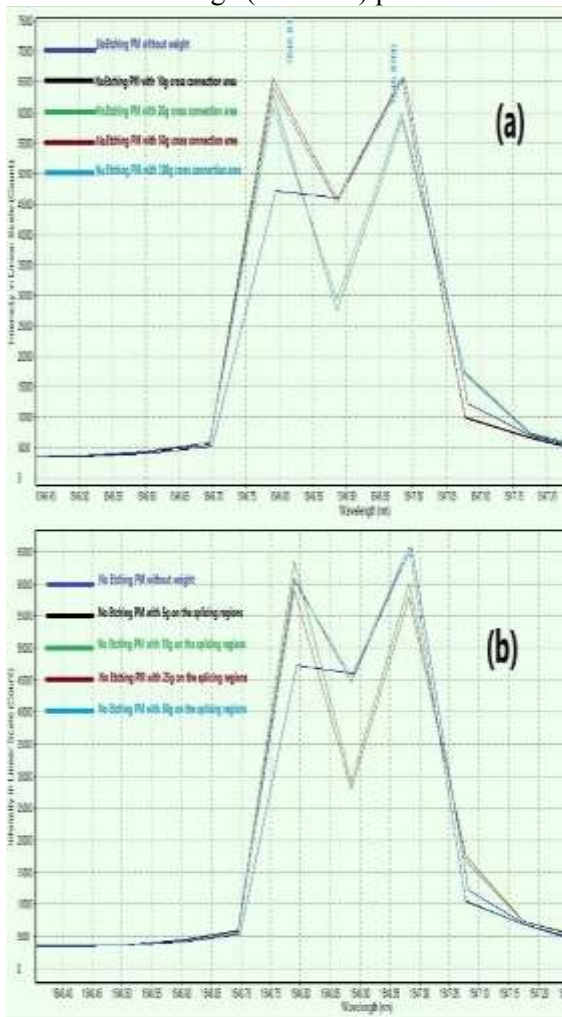




**Figure (4):** for PMF without etching connected to Sagnac loop adding to (a) weights on cross sectional area (b) weights on the splicing regions
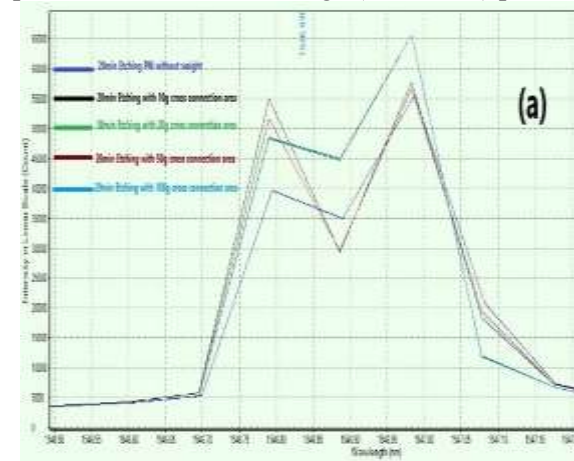
The second case using the PM with etching 10min and applied the mechanical stress as shown in figure (5) which show signals and FHWM of dual band pass filter in the range (123
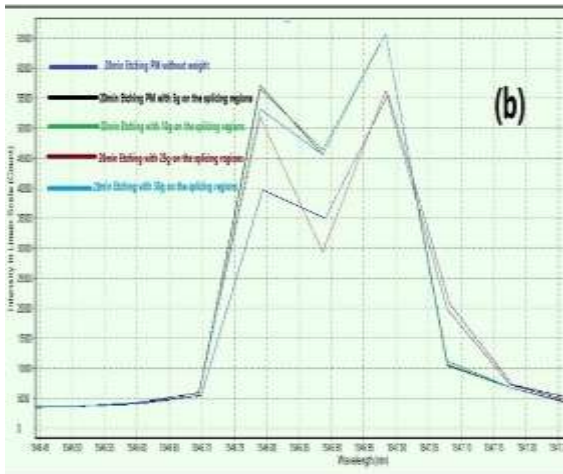
– 293) pm, and notch filter in range (90 – 115) pm.





**Figure (5):** for PMF 10min etching connected to Sagnac loop adding to (a) weights on cross sectional area (b) weights on the splicing regions.

The third case using the PM with etching 20min and applied the mechanical stress as shown in figure (6) which show signals and FHWM of dual band pass filter in the range (137 – 315) pm, and notch filter in range (102 – 125) pm.



.

**Figure (6):** for PMF 20min etching connected to Sagnac loop adding to (a) weights on cross sectional area (b) weights on the splicing regions.
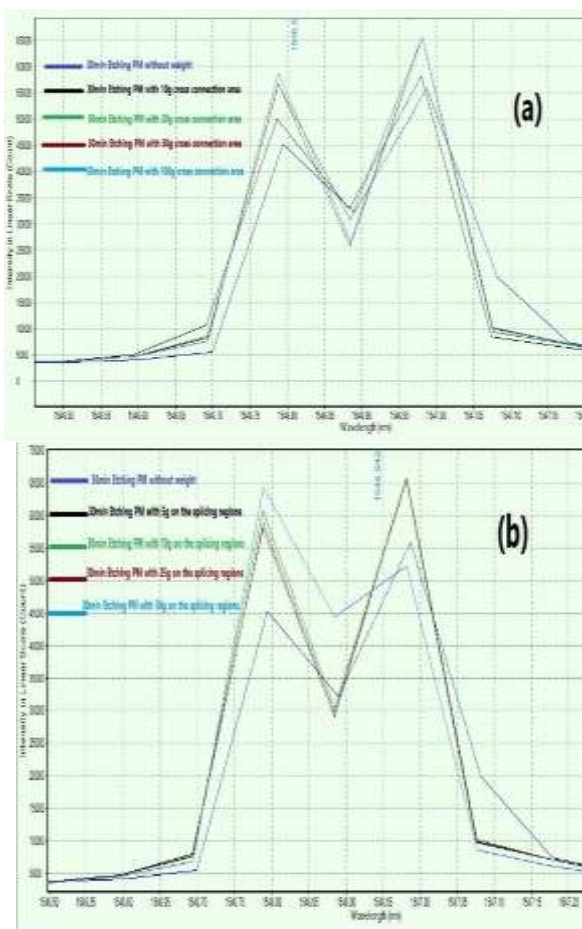
The forth case using the PM with etching 30min and applied the mechanical stress as shown in figure (7) which show signals and FHWM of dual band pass filter in the range (130 – 308) pm, and notch filter in range (99 – 122) pm.



**Figure (7):** for PMF 30min etching connected to Sagnac loop adding to (a) weights on cross sectional area (b) weights on the splicing regions.

When applied weight on cross sectional area of PM as part of MZI in the loop of hypbrid Sagnac interferomerter will get many results for FWHM( by tuning weights and etching). These results of FWHM will be increased by increasing etching time at the same weights.

Regarding applied weights on both splicing regions will get maximum result for FWHM at the same weights for PM with 20min etching , each of these results are summarized in the figure (8).
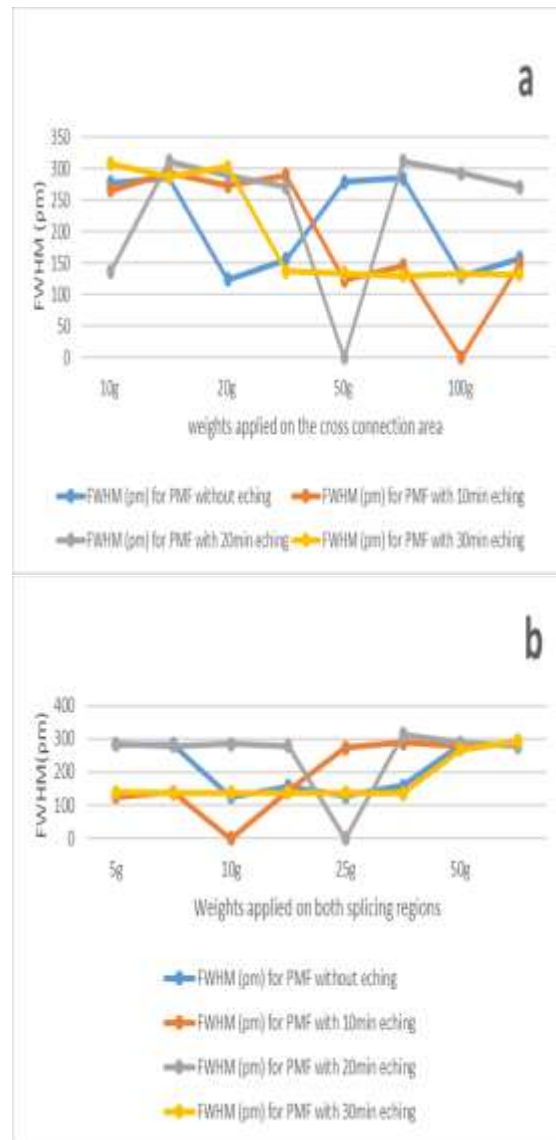


**Figure (8)**: The Full Width Half Maximum variation of HIS which contained PM-MZI as loop (a) for weights apply on cross sectional area (b) for weights apply on the both splicing regions.

The peak wavelength is changed by tuning of etching adding to other parameters which contained weights and get two peaks and involving notch between them , these peaks will

5

be in different values from (1546.808 nm - 1546.972 nm) , each of these results are summarized in the figure (9).
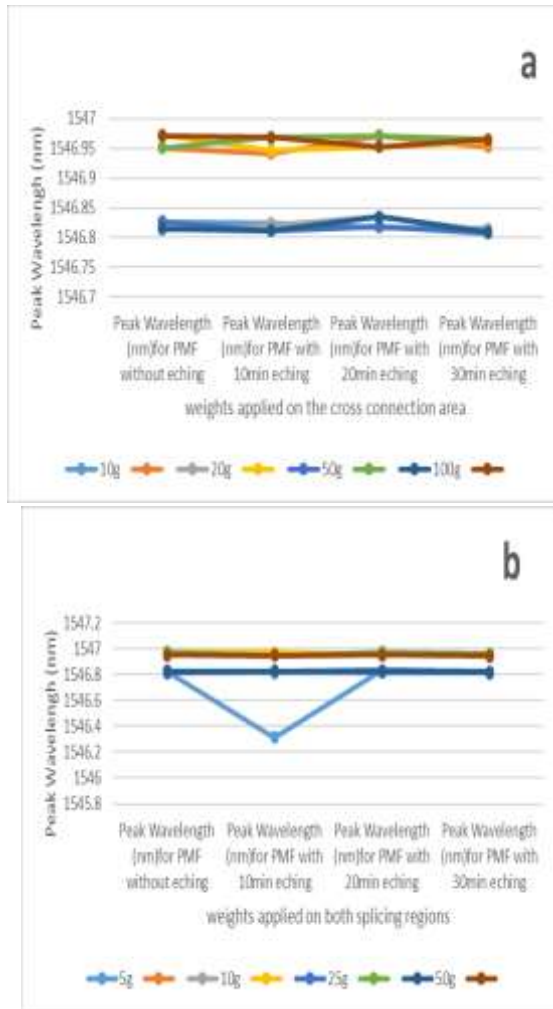




**Figure (9)**: The peak wavelength variation of HIS which contained PM-MZI as loop (a) for weights apply on cross connection area (b) for weights apply on the both splicing regions.

In this paper took etching 10 min for PMF and make relation for result between forces (N) and the strain as show in figure (10)

The FWHM results of notch filter at 10 min etching with weights on cross connection area are summarized in table (3).
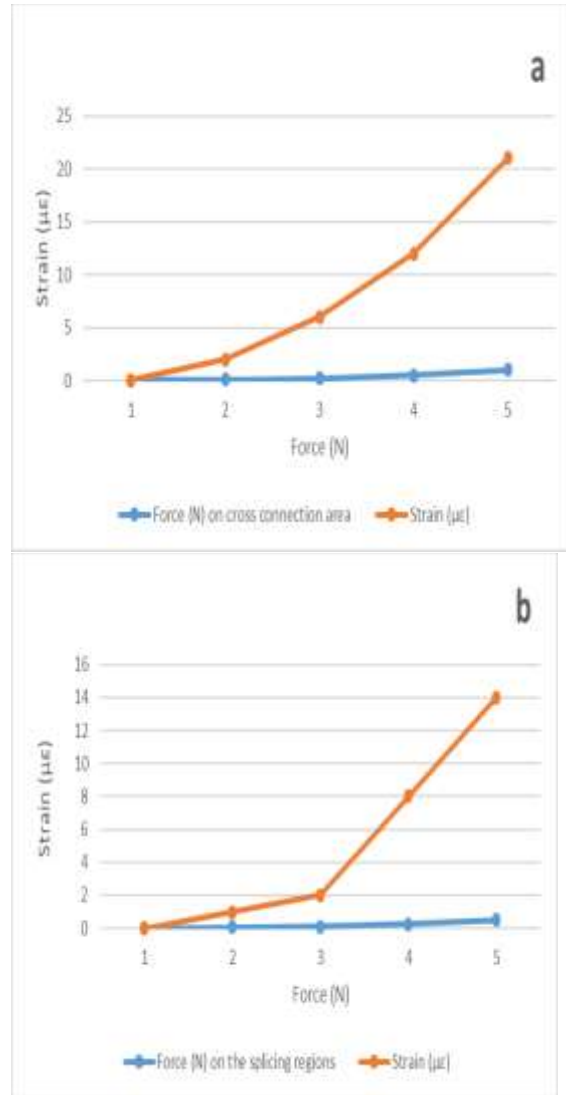




**Figure (10)**: The relation between Mechanical force and strain ($\mu\varepsilon$) (a) for weights apply on cross connection area (b) for weights apply on the both splicing regions.

**Table (3):** FWHM of notch filter with respect to weights on cross connection area.

| Weights on cross connection area  (g) | FWHM (pm) for of notch filter |
|---|---|
| 10 | 125 |
| 20 | 128 |
| 50 | 98 |
| 100 | 90 |

The FWHM results of notch filter at 10 min etching with weights on splicing regions are summarized in table (4).

**Table (4):** FWHM of notch filter with respect to weights on splicing regions.

| Weights on splicing regions (g) | FWHM (pm) for of notch filter |
|---|---|
| 5 | 99 |
| 10 | 90 |
| 25 | 132 |
| 50 | 134 |

The FWHM results of dual band pass filter at different duration of etching with weights on cross connection area are summarized in table (5).

**Table (5):** the result of FWHM of weights applied on cross connection area with different etching.

| Weights on cross area (g) | FWHM at no etching (pm) | FWHM at 10 min (pm) | FWHM at 20min (pm) | FWHM at 30min (pm) |
|---|---|---|---|---|
| 10 | 278 | 266 | 137 | 308 |
| | 286 | 293 | 312 | 287 |
| 20 | 127 | 273 | 290 | 303 |
| | 156 | 290 | 271 | 137 |
| 50 | 279 | 141 | 315 | 134 |
| | 285 | 146 | 314 | 130 |
| 100 | 129 | 123 | 293 | 133 |
| | 158 | 124 | 271 | 132 |

The FWHM results of dual band pass filter at different duration of etching with weights on splicing regions are summarized in table (6).

**Table (6):** the result of FWHM of weights applied on splicing regions with different etching.

| weights on splicing regions (g) | FWHM at no etching (pm) | FWHM at 10 min (pm) | FWHM at 20min (pm) | FWHM at 30min (pm) |
|---|---|---|---|---|
| 5 | 282 | 127 | 285 | 139 |
| | 283 | 139 | 279 | 135 |
| 10 | 126 | 123 | 284 | 137 |
| | 157 | 124 | 278 | 138 |
| 25 | 129 | 274 | 315 | 138 |
| | 159 | 288 | 314 | 136 |
| 50 | 282 | 276 | 288 | 267 |
| | 282 | 287 | 276 | 294 |

The highest peak power intensity value in watt per square meter was recorded result in the case of no etching is 74564.513 which equal to (914.58 µW) as peak power, in case of 10min etching (977.36 µW) in case of 20min (914.857 µW) and in case of 30min (933.635 µW), the figure (11) show the peak power of HIS which contained PM-MZI as loop after applying different values of mechanical forces as different weighs applied on cross and splicing regions.
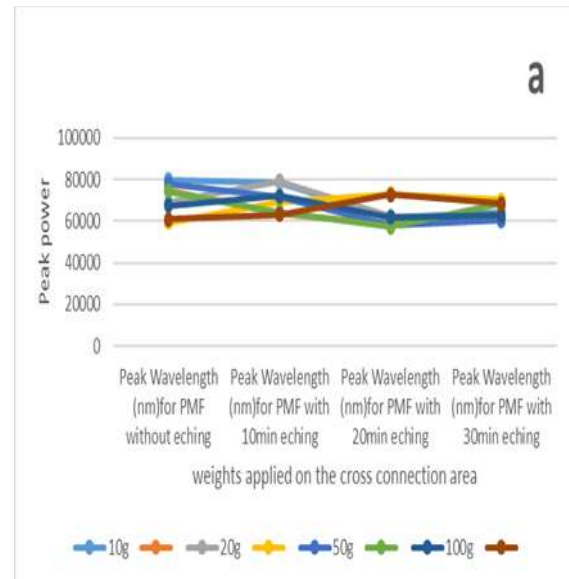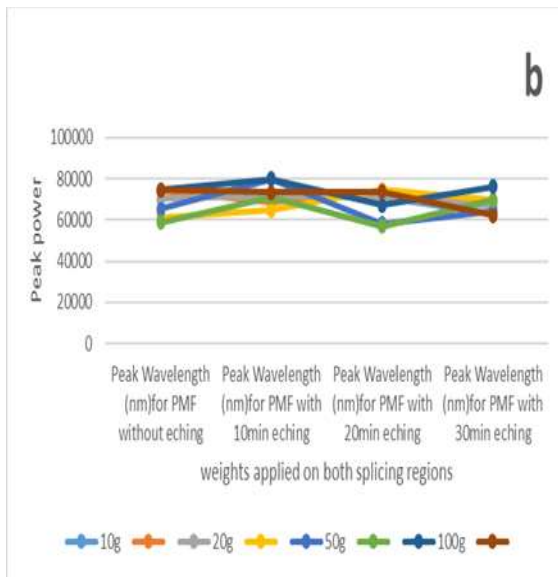
**Figure (11)**: The peak power intensity variation of HIS which contained PM-MZI as loop (a) for weights apply on cross connection area (b) for weights apply on the both splicing regions.

## 4. **Conclusion**

In conclusion; a simple structure, low cost all optical notch pass filter was designed and the main point that the better filter with narrow FWHM for dual band pass filter and notch filter can be obtained by using hybrid Sagnac interferometer with MZI of PM as a loop with etching 10 min and affected by weights 100g (Force 0.98 N) on cross sectional area or by weights 10g (Force 0.098) on both splicing regions equal to 123 pm and 90 pm, respectively. These results are promising to make possible the acquisition of narrowband pass filters and slit filters for telecom applications. When the FWHM decrease in the frequency domain as it is increasing in the time domain that occurs because there is an inverse relationship between frequency and time. The average power decreased with increase the duration of etching PM in MZI due to change in FWHM of the output signal. It can be used in all optical integrated signal processing devices to reduce the electronics and their characteristics noise there by achieving higher data processing and transmission rates.

## **References**

[1] K. Agrawal, G.P. "*Application of Nonlinear Fiber Optics*", 2nded. Academic Press: New York, (2001).

[2] D. V. Skryabin, "*Coupled core-surface solitons in photonics crystal fibers*," Opt. Express 12, 4841–4846 (2004).

[3] B. Lee, Young Ho Kim 1, Kwan Seob Park, Joo Beom Eom, Myoung Jin Kim, Byung Sup Rho and Hae Young Choi "*Interferometric Fiber Optic Sensors*" Sensors, vol:12, PP.10430-10449, (2012)

[4] S. Korposh, Stephen W. James, Seung-Woo Lee and Ralph P. Tatam "*Tapered Optical Fibre Sensors: Current Trends and Future Perspectives*", Sensors, vol. 19, No. 2294, (2019).

[5] Wu, Shun, et al. "*Temperature-independent ultra-sensitive refractive index sensor based on hollow-core silica tubes and tapers.*" Optics Express 29.7, PP. 10939-10948, (2021).

[6] Wang, Jin, et al. "*Temperature insensitive fiber Fabry-Perot/Mach-Zehnder hybrid interferometer based on photonic crystal fiber for transverse load and refractive index measurement.*" Optical Fiber Technology 56, No.102163, (2020).

[7] Peng, Wei, et al. "*Miniature fiber-optic strain sensor based on a hybrid interferometric structure.*" IEEE Photonics Technology Letters 25.24, PP. 2385-2388 (2013).

[8] Yi, Liu, and Yu Changyuan. "*Highly stretchable hybrid silica/polymer optical fiber sensors for large-strain and high-temperature application.*" Optics express 27.15, PP. 20107-20116, (2019).

[9] Zhao, Ping, Lei Shi, and Xinliang Zhang. "*Single-notch filter based on a compact asymmetric microfiber coupler.*" CLEO: QELS Fundamental Science. Optical Society of America, 2013.

[10] J. Yang, Y. Zheng, L. H. Chen, C. C. Chan, X. Dong, P. P. Shum, and H. Su, "*Miniature temperature sensor with germania-core optical fiber*" Opt. Express 23(14), PP.17687–17692, (2015).

[11] Zhao, Yong, et al. "*A ring-core optical fiber sensor with asymmetric LPG for highly sensitive temperature measurement.*" IEEE Transactions on Instrumentation and Measurement 66.12, PP. 3378-3386, (2017).

[12] Xu, Zhilin, et al. "*Investigation of temperature sensing characteristics in selectively infiltrated photonic crystal fiber.*" Optics express 24.2, PP.1699-1707, (2016).

[13] Wu, Zhifang, et al. "*Supermode Bragg grating combined Mach-Zehnder interferometer for temperature-strain*

*discrimination*." Optics express 23.26, PP.33001-33007, (2015).

[14] Zhang, Zhe, et al. "*Hollow-core-fiber-based interferometer for high-temperature measurements*." IEEE Photonics Journal 9.2, PP.1-9, (2017).

[15] Yang, Jingyi, et al. "*Magnetic field sensing with reflectivity ratio measurement of fiber Bragg grating*." IEEE Sensors Journal 15.3, PP. 1372-1376, (2014).

[16] V. Bhatia and A. M. Vengsarkar, "*Optical fiber long-period grating sensors*," Opt. Lett. 21(9), PP.692–694, (1996).

[17] F. M. Abdulhussein, M. Hou, S. Liu, T. S. Mansour, and P. Lu, "*Integrated FabryPerot/Fiber Bragg Grating Sensor for Simultaneous Measurement*" in CLEO: 2015, OSA Technical Digest (online) (Optical Society of America, (2015) .

[18] T. S. Mansour and F.M. Abdulhussein, "*Dual Measurements of Pressure and Temperature With Fiber Bragg Grating Sensor*", Vol.11,pp.86-91,(2015).

[19] T. Zhu, T. Ke, Y. Rao, and K. S. Chiang, "*Fabry-Perot optical fiber tip sensor for high temperature measurement*," Opt. Commun. 283(19), 3683–3685 (2010).

[20] Y. Zhang, L. Yuan, X. Lan, A. Kaur, J. Huang, and H. Xiao, "*High-temperature fiber-optic Fabry-Perot interferometric pressure sensor fabricated by femtosecond laser*," Opt. Lett. 38(22), 4609–4612 (2013).

[21] L. Jiang, J. Yang, S. Wang, B. Li, and M. Wang, "*Fiber Mach-Zehnder interferometer based on microcavities for high-temperature sensing with high sensitivity*," Opt. Lett. 36(19), 3753–3755 (2011).

[22] J. Zhu, A. Zhang, T.-H. Xia, S. He, and W. Xue, "*Fiber-optic high-temperature sensor based on thin-core fiber modal interferometer*," IEEE Sens. J. 10(9), 1415–1418 (2010).

[23] Abdulwahhab, A. A., and T. S. Mansour. "*Design and Analysis of BIMD Double Clad MMF -MZI Using Optiwave Simulation*". Iraqi Journal of Laser, vol. 20, no. 1, Aug. 2021, pp. 1-5, (2021).

[24] Y. Liu, B. Liu, X. Feng, W. Zhang, G. Zhou, S. Yuan, G. Kai, and X. Dong, "*High-birefringence fiber loop mirrors and their applications as sensors*," Appl. Opt. 44(12), 2382–2390 (2005).

[25] Mansour, T. S., and D. H. Abbass. "*Chemical Sensor Based on a Hollow-Core Photonic Crystal Fiber*". Iraqi Journal of Laser, vol. 12, no. A, pp. 37-42, (2015).

[26] Noori, Nada F., and Tahreer S. Mansour. "*Design and Construction of Tunable Band Pass Filter Using Hybrid FPMZI*." Design Engineering, 6959-6972, (2021).

[27] B. H. Mutar ,N. Faris, Y. I. Hammadi and T. Mansour, "*In-Line Fiber Tunable Pulse Compressor using PM-Mach Zehnder Interferometer*" Journal of Mechanical Engineering Research and Developments. Vol. 44, pp. 287-297, (2021).

[28] Mutar, B. H., and T. S. Mansour. "*Design of Tunable Optical Band Pass Filter Based on in-Line PM-Mach Zehnder Interferometer*". Iraqi Journal of Laser, vol. 20, no. 1, pp. 6-12, (2021).

**تنغيم مرشحات النطاق البصري بواسطة سانياك باستخدام الالياف الضوئية المحافظة على الاستقطاب المحفورة**

**ريسان محي الدين طاهر        تحرير صفاء منصور**

معهد الليزر للدراسات العليا / جامعة بغداد – بغداد / العراق

**الخلاصة:** في هذا العمل، تم تقديم مرشح تمرير النطاق المتباين المستند  ضمن دائرة السانياك وتحتوي دائرته على مقياس التداخل المتراصف المحافظ على الاستقطاب من نوع ماخ – زندر لكي تعمل كتوليف لعملية انتاج مرشح النطاق البصري الضيق. تم تقشير 10سم من هذا الليف (PMF) و ربطه بين جزأين من  الالياف احادية النمط من نوع  (SMF-28) بطول (12سم ) للكل ليف وربطهما بأستخدام تقنيه اللحام الكهربائي و قد تم ازاله جزء من قطر اليف (PMF) بواسطة  حامض الهايدروفلوريك أسد وبتركيز 40% وعلى ثلاث مراحل بفترات متزايدة بمقدار 10ثانيه بالاضافة لعمل توليف بواسطة الاوزان المختلفة على مركز الليف (PMF)  وكذلك عل مناطقتين اللحام الجانبية، وقد تم الحصول عل مرشح بصري ضيف  وبمديات مختلفة حسب التوليف ولكن تم تثبيت افضل  قياس  في مرحلة الازالة لمدة 10 ثواني مع تسليط اوزان بقيمة 100غرام عل المنطقة الوسطية لليف او 10 غرام علي منطقتي اللحام وتسجيل مقدار اضيق مقدار للمرشح و مقدار عرض الموجة   FWHM مساويا 123 بيكو متر للمرشحات المزدوجة و 90 بيكو متر لمرشح الشق. علما ان مصدر اليزر النبضي المستخدم في هذا العمل له ذروة تبلغ 1.2296 ملي واط، FWHM 286 بيكو متر، ويتركز عند الطول الموجي 1546.7 نانومتر.